Study on vehicle driving state and parameters estimation based on triple cubature Kalman filter

Gang Li*

Automobile and Transportation Engineering College,
Liaoning University of Technology,
Liaoning Jinzhou, 121001, China
Email: qcxyligang@lnut.edu.cn
*Corresponding author

Dong-sheng Fan, Ye Wang and Rui-chun Xie

Automobile and Transportation Engineering College,
Liaoning University of Technology,
Liaoning Jinzhou, 121001, China
Email: 771304328@qq.com
Email: 1029153923@qq.com
Email: 1377936790@qq.com

Abstract: For the problem of vehicle driving state and parameters estimation in the process of vehicle driving, the vehicle state and parameters estimation algorithms are studied based on the triple cubature Kalman filter. The nonlinear three degrees of freedom model with Dugoff tyre model is established. The vehicle driving state estimator, road adhesion coefficient estimator and vehicle parameters estimator are designed based on the theory of triple cubature Kalman filter. To estimate the driving state and parameters accurately, the three estimators connect to each other in the process of the estimation and form a closed-loop feedback in real time. The estimation algorithms are verified based on the driving simulator. The serpentine docking road conditions with changing speed are selected to verify the estimation algorithms based on the driving simulator in-loop simulation test. The experiments' results show that the vehicle driving state and parameters are estimated accurately by the estimation algorithms.

Keywords: Dugoff tyre; driving simulator in-loop simulation experiment; road friction coefficient; triple cubature Kalman filter; vehicle driving state; vehicle parameters.

Reference to this paper should be made as follows: Li, G., Fan, D-S., Wang, Y. and Xie, R-C. (2020) 'Study on vehicle driving state and parameters estimation based on triple cubature Kalman filter', *Int. J. Heavy Vehicle Systems*, Vol. 27, Nos. 1/2, pp.126–144.

Biographical notes: Gang Li received his MS in Vehicle Engineering from Liaoning University of Technology, Jinzhou, China, in 2006, and the PhD in Vehicle Engineering from Jilin University, Changchun, China, in 2013, and is currently a Professor and Vice-Dean of the College of Automobile and Traffic Engineering, Liaoning University of Technology, Jinzhou, China. He has

authored or co-authored more than 50 journal and conference papers, and was the recipient of 30 China patents and software copyrights. He is in charge of numerous projects funded by national government and institutional organisations on electric vehicles and energy management systems. His current research interests include model, simulation, intelligent control for vehicles and vehicle active safety.

Dong-sheng Fan is a graduate student at Liaoning University of Technology and will graduate in 2020.

Ye Wang received the MS in Vehicle Engineering from Liaoning University of Technology, Jinzhou, China, in 2018, and he is working in Wuhan.

Rui-chun Xie received his MS in Vehicle Engineering from Liaoning University of Technology, Jinzhou, China, in 2015, and he is working in Shanghai.

1 Introduction

The vehicle handling stability can be effectively improved and the occurrence of traffic accidents can be reduced through using vehicle active safety control system. It is necessary to obtain vehicle driving state and parameters accurately in real-time for vehicle active safety control. While the costs of vehicle speed and road directly identify technology are expensive, so the estimation for vehicle state and parameters has become popular in the field of vehicle dynamics and control using low-cost sensors and relative theory (Antonova et al., 2011; Baffet et al., 2007; Best, 2009; Choi et al., 2013; Crassidis and Markley, 2003; Grip et al., 2008; Gunnarsson et al., 2002; Gust, 2010; Julier and Uhlman, 2004; Kandepu and Foss, 2008; Kim, 2009; Nam and Fujimoto, 2012; Phanomchoeng et al., 2011; Wenzel et al., 2006; Wilkin et al, 2006; Zong et al., 2011).

One estimation method for lateral speed which adopts the road adhesion conditions is proposed by Grip et al. (2008), and its stability is analysed. But the method can obtain better estimation result only under changing driving conditions (Grip et al., 2008). In another paper (Phanomchoeng et al., 2011), the cheap sensors are used by Griddsada Braghin, and a new nonlinear observer is designed to estimate vehicle side-slip angle, by using average theory to express nonlinear error dynamics with convex combination time-varying coefficient matrix. The vehicle tyre model is used (Choi et al., 2013) to describe the dynamic coupling characteristics for the tyre longitudinal and lateral movement, and the linear recursive least squares method is used to estimate the road adhesion coefficient. Nowadays, the extended Kalman filter (Baffet et al., 2007; Best, 2009; Kim, 2009; Nam and Fujimoto, 2012; Wenzel et al., 2006; Wilkin et al., 2006; Zong et al., 2011), unscented Kalman filter (Antonova et al., 2011; Crassidis and Markley, 2003; Julier and Uhlman, 2004; Kandepu and Foss, 2008) and particle filter algorithm (Gust, 2010; Gunnarsson et al., 2002) are mainly used for vehicle state estimate and road adhesion coefficient estimate. Vehicle state with nonlinear factors can be estimated through using extended Kalman filtering (EKF). In another paper (Baffet et al., 2007), based on Burckhardt/Kiencke model, the vehicle driving state and tyre friction forces are estimated through using EKF theory. Other authors (Nam and Fujimoto, 2012) proposed that vehicle tyre forces are measured directly in real-time by using tyre force

measuring instrument. The least squares method with multiple forgetting factor and EKF are respectively used to estimate vehicle side-slip angle and vehicle roll angle. Elsewhere (Zong et al., 2011), the dual extended Kalman filter (DEKF) technique is proposed to estimate the vehicle states and the road adhesion coefficient synchronously. The complex Jacobian matrices are needed to solve when used the EKF algorithm, so the errors will be caused easily and the real-time performance of estimator will be reduced (Pengov et al., 2001). The unscented Kalman filter (UKF) approximates to the state of probability density function based on unscented transform (UT). Its computing accuracy is higher than EKF algorithm (Satria and Best, 2005; Van Der Merwe et al., 2004). In another paper (Antonova et al., 2011), the three degrees of freedom based on the magic type tyres is used. The vehicle driving state and tyre state are estimated by UKF filter that additionally considers the vertical tyre stiffness. But the Gaussian approximation method of UKF cannot meet the accuracy requirement of vehicle dynamic controller when dealing with strongly nonlinear problems (Julier and Uhlman, 2004; Julier et al., 2000). The particle filter has a unique advantage in dealing with the nonlinear or non-Gaussian system problems, but the particle filter has problems with fewer particle samples and poor real-time performance (Givon et al., 2009).

Cubature Kalman filter (CKF) is a new type of nonlinear Gaussian filtering, put forward by Canada scholars in the year of 2009, and it has strictly mathematical derivation (Arasaratnam et al., 2009, 2010). It uses numerical integration to approximate the weighted Gaussian-integral based on third-order cubature rules. It makes full use of the high efficiency characteristics of cubature integral to calculate multi-dimensional function integral. CKF has $2n$ (n represents the state dimension) cubature points with equal weights, it has been proved that the accuracy of probability distribution is better than UKF after nonlinear transformation (Li and Sun, 2013). So the CKF is chosen to estimate the vehicle state and parameters in this paper.

At present, the estimators which based on models are widely used among the vehicle state estimation methods, but they are too dependent on the accuracy of the model parameters. Assuming that the vehicle parameters (such as moment of inertia, vehicle mass, and centroid position, etc.) are known and have constant values, these approximation values of vehicle parameters can be obtained by measuring. However, these parameters will change with different working conditions in the process of the vehicle driving. For example, for passenger bus, no-load and full-load will evidently affect the vehicle mass. For large trucks, no-load and full-load will significantly influence the centroid position of vehicle and the moment of inertia. Therefore, it is very important to consider the uncertainty of vehicle parameters when estimating the vehicle state. Only by constantly adjusting the uncertainty of vehicle parameters when estimating the vehicle state, can the vehicle driving information be obtained more accurately.

The nonlinear three degrees of freedom (3-DOF) model and Dugoff tyre model are adopted as the vehicle driving state estimation models. The vehicle state variables such as longitudinal/lateral velocity and so on are estimated based on CKF theory. And the road adhesion coefficient is estimated by using state estimate value and sensor measurement value. At the same time, the vehicle mass, the moment of inertia about z-axis and the centroid position of vehicle to front axle are estimated using the vehicle state, road adhesion coefficient estimation values and sensor information. When the estimate consequence of vehicle state and parameters estimator can meet the requirements, then the driving state and the parameters estimator are set up. To realise the estimate information correcting each other at one time and adaptive adjustment, in order to

accurately estimate vehicle driving state, road adhesion coefficient and vehicle parameters. Since the error covariance matrix will lose positive definiteness because of the errors such as calculation round off error, the singular value decomposition (SVD) is put forward in the paper instead of Cholesky decomposition to solve the problem that error covariance matrix is non-positive matrix. Finally, the estimate algorithm is verified by driving simulator in-loop experiments.

2 Vehicle estimation model

2.1 Nonlinear 3-DOF vehicle dynamics model

3-DOF vehicle dynamics model is adopted as vehicle estimation model. By using the simplified estimation model, the nonlinear 3-DOF vehicle dynamics model which includes yaw, longitudinal and lateral is setup. The nonlinear 3-DOF model is shown in Figure 1, and the following assumptions are made:

- the mass centre of vehicle estimation model coincides with the origin of vehicle coordinate system
- the effect of suspension for vehicle vertical movement is ignored
- the vehicle does not have the freedom of pitch and roll direction
- the effect of longitudinal rolling resistance for state parameter estimation is ignored.

In Figure 1, a is the distance from the centre of centroid position to the front axle, b is the distance from the centre of centroid position to the rear axle, t_f is the front wheel tread, t_r is the rear wheel tread, $\alpha_{fl,fr}$ are tyre side-slip angle of left front wheel and right front wheel, $\alpha_{rl,rr}$ are tyre side-slip angle of left rear wheel and right rear wheel, $F_{x\_fl,fr,rl,rr}$ are respectively corresponding to the longitudinal force of wheel, $F_{y\_fl,fr}$ are respectively corresponding to the lateral forces of front wheel, $\delta_{fl,fr}$ are wheel angle of left front wheel and right front wheel respectively.

Figure 1 Nonlinear 3-DOF model

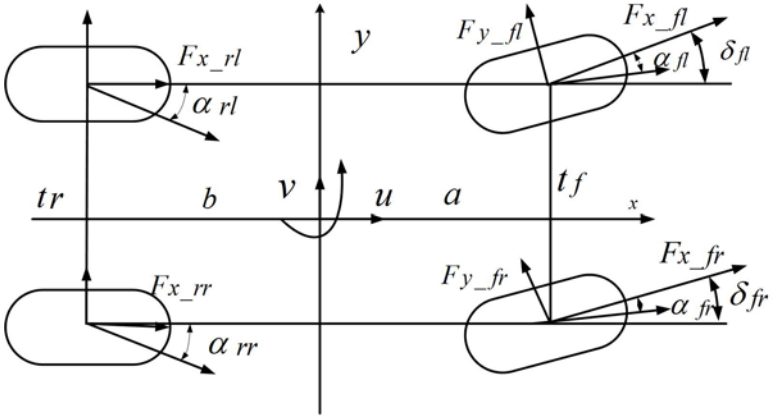

The dynamics equations of 3-DOF vehicle model are as follows:

$$\dot{u} = a_x + v.r \tag{1}$$

$$\dot{v} = a_y - ur \tag{2}$$

$$\dot{r} = \frac{1}{I_z}\Gamma \tag{3}$$

where, u is the vehicle longitudinal velocity, v is the lateral velocity, r is the vehicle yaw rate, a_x is the longitudinal acceleration, a_y is the lateral acceleration, Γ is the yaw moment, I_Z is the moment of inertia about z-axis. Based on the dynamics equation, other parameters are calculated by:

$$\begin{aligned}\Gamma = {} & a(F_{x\_fl}\sin\delta_{fl} + F_{y\_fl}\cos\delta_{fl}) - \frac{t_f}{2}(F_{x\_fl}\cos\delta_{fl} - F_{y\_fl}\sin\delta_{fl}) \\ & + a(F_{x\_fr}\sin\delta_{fr} + F_{y\_fr}\cos\delta_{fl}) + \frac{t_f}{2}(F_{x\_fr}\cos\delta_{fr} - F_{y\_fr}\sin\delta_{fr}) - bF_{x\_rl} \\ & - \frac{t_r}{2}F_{x\_rl} - bF_{x\_rr} + \frac{t_r}{2}F_{x\_rr}\end{aligned} \tag{4}$$

$$a_x = \frac{1}{m}(F_{x\_fl}\cos\delta_{fl} - F_{y\_fl}\sin\delta_{fl} + F_{x\_fr}\cos\delta_{fr} - F_{y\_fr}\sin\delta_{fr} + F_{x\_rl} + F_{x\_rr}) \tag{5}$$

$$a_y = \frac{1}{m}(F_{x\_fl}\sin\delta_{fl} + F_{y\_fl}\cos\delta_{fl} + F_{x\_fr}\sin\delta_{fr} + F_{y\_fr}\cos\delta_{fr} + F_{x\_rl} + F_{x\_rr}) \tag{6}$$

$$\beta = \frac{v}{u} \tag{7}$$

$$\begin{aligned}\alpha_{fl,fr} &= \delta_{fl,fr} - \arctan\left(\frac{v + ar}{u \pm \frac{t_f}{2}r}\right) \\ \alpha_{rl,rr} &= \delta_{rl,rr} - \arctan\left(\frac{-v + br}{u \pm \frac{t_r}{2}r}\right)\end{aligned} \tag{8}$$

$$\begin{aligned}v_{fl,fr} &= \sqrt{\left(u \mp \frac{t_f}{2}r\right)^2 + (v + ar)^2} \\ v_{rl,rr} &= \sqrt{\left(u \mp \frac{t_r}{2}r\right)^2 + (v - br)^2}\end{aligned} \tag{9}$$

$$\begin{aligned} F_{z\_fl,fr} &= \left(\frac{1}{2}mg \pm ma_y \frac{h}{t_f}\right)\frac{b}{l} - \frac{1}{2}ma_x\frac{h}{l} \\ F_{z\_rl,rr} &= \left(\frac{1}{2}mg \pm ma_y \frac{h}{t_r}\right)\frac{b}{l} + \frac{1}{2}ma_x\frac{h}{l} \end{aligned} \tag{10}$$

where β is vehicle side-slip angle, m is the vehicle mass; h is the height of the centre of mass; l for the front and rear wheelbase, $v_{fl,fr}$ are wheel centre speed of left and right front wheel respectively, $v_{rl,rr}$ are wheel centre speed of left and right rear wheel respectively, $F_{z\_fl,fr}$ are vertical load of left and right front wheel respectively, $F_{z\_rl,rr}$ are vertical load of left and right rear wheel respectively.

2.2 Dugoff tyre model

The longitudinal and lateral forces on the tyres are calculated through using Dugoff tyre model. For each wheel, the longitudinal and lateral force can be expressed by the following formula.

$$F_{x\_ij} = \mu_{\_ij} F_{z\_ij} c_x \frac{\lambda_{\_ij}}{1-\lambda_{\_ij}} f(L) \tag{11}$$

$$F_{y\_ij} = \mu_{\_ij} F_{z\_ij} c_y \frac{\tan(\alpha)}{1-\lambda_{\_ij}} f(L) \tag{12}$$

In which,

$$f(L) = \begin{cases} L.(2-L), & L<1 \\ 1, & L \geq 1 \end{cases} \tag{13}$$

$$L = \frac{1}{2\sqrt{C_x^2\lambda_{\_ij}^2 + C_y^2\tan^2\alpha}}(1-\lambda_{\_ij}).(1-\varepsilon.u.\sqrt{C_x^2\lambda_{\_ij}^2 + C_y^2\tan^2\alpha}) \tag{14}$$

Slip ratio can be divided into braking and driving two cases.

$$\begin{aligned} \lambda_{ij} &= \frac{R_e\omega_{ij} - v_{ij}}{v_{ij}} = \frac{R_e\omega_{ij}}{v_{ij}} - 1 < 0 \quad \text{(Braking)} \\ \lambda_{ij} &= \frac{R_e\omega_{ij} - v_{ij}}{R_e\omega_{ij}} = 1 - \frac{v_{ij}}{R_e\omega_{ij}} > 0 \quad \text{(Driving)} \end{aligned} \tag{15}$$

where $\mu_{\_ij}$ is the road adhesion coefficient, $\lambda_{\_ij}$ is longitudinal slip ratio, C_y is tyre cornering stiffness, C_x is tyre longitudinal slip stiffness, R_e is the wheel rolling radius, ε is the impact factor of speed, F_{x_ij} are tyre longitudinal forces, F_{y_ij} are tyre lateral forces, i, j are the location of tyres, i is the front or rear wheel, j is the left or right wheel.

3 Design for driving state and parameter algorithm

The Dugoff tyre model is adopted, and the nonlinear 3-DOF model is established. The driving state and parameters estimator are designed based on triple CKF theory, its specific algorithm such as equations (16)–(54).

(1) Time update of road adhesion coefficient estimation

① Through SVD to obtain the square root of the covariance matrix $P_p(k-1)$

$$P_p(k-1) = A_p(k-1)\Lambda_p(k-1)A_p^T(k-1) \tag{16}$$

where the row of the $A_p(k-1)$ is unit orthogonal feature vector of the error covariance $P_p(k-1)$, $\Lambda_p(k-1)$ is the diagonal matrix, $\Lambda_p(k-1) = diag[S_{p1}^2, S_{p2}^2 ..... S_{pN}^2]$, S_{pi} are eigen values of the error covariance matrix.

$$X_{pj}(k-1) = A_{pi}(k-1)S_{pi}(k-1)\xi_{pj} + X_p^{\wedge}(k-1) \tag{17}$$

where the cubature points $\xi_{a,j} = \sqrt{v/2}[1]_{p,j}$, $[1]_{pj}$ represents the jth element of the cubature point sets, M is the total cubature point. When using third-order cubature principle, the total cubature point of M is twice the number of state dimensional-N, $i = 1, 2 \ldots N$, $j = 1, 2 \ldots M$. Among of the parameter variables, $N = 4$, the cubature point set as follows:

$$\left\{ \begin{bmatrix} 1 \\ 0 \\ 0 \\ 0 \end{bmatrix}, \begin{bmatrix} 0 \\ 1 \\ 0 \\ 0 \end{bmatrix}, \begin{bmatrix} 0 \\ 0 \\ 1 \\ 0 \end{bmatrix}, \begin{bmatrix} 0 \\ 0 \\ 0 \\ 1 \end{bmatrix}, \begin{bmatrix} -1 \\ 0 \\ 0 \\ 0 \end{bmatrix}, \begin{bmatrix} 0 \\ -1 \\ 0 \\ 0 \end{bmatrix}, \begin{bmatrix} 0 \\ 0 \\ -1 \\ 0 \end{bmatrix}, \begin{bmatrix} 0 \\ 0 \\ 0 \\ -1 \end{bmatrix} \right\}$$

② The cubature point $X_{pj}^*(k/k-1)$

$$X_{pj}^*(k/k-1) = f(X_{pj}(k-1)) \quad j = 1, 2, \ldots, M \tag{18}$$

③ The parameter variables $X_p^{\wedge}(k/k-1)$

$$X_p^{\wedge}(k/k-1) = \sum_{j=1}^{M} \frac{1}{M} X_{pj}^*(k/k-1) \tag{19}$$

④ The error covariance matrix $P_p(k/k-1)$

$$P_p(k/k-1) = \sum_{j=1}^{M} \frac{1}{M} \omega_{pj} X_{pj}^*(k/k-1) X_{pj}^{*T}(k/k-1) - X_p^{\wedge}(k/k-1) X_p^{\wedge T}(k/k-1) + Q_p \tag{20}$$

(2) Time update of vehicle parameters estimator

① Through SVD to obtain the square root of the covariance matrix $P_t(k-1)$

$$P_t(k-1) = A_t(k-1)\Lambda_t(k-1)A_t^T(k-1) \tag{21}$$

where the row of the $A_t(k-1)$ is unit orthogonal feature vector of the error covariance $P_{t(k-1)}$, $\Lambda_t(k-1)$ is the diagonal matrix, $\Lambda_t(k-1) = diag[S_{t1}^2, S_{t2}^2 ....., S_{te}^2]$, S_{ti} are eigen values of the error covariance matrix $P_t(k-1)$.

$$X_{tj}(k-1) = A_{ti}(k-1)S_{ti}(k-1)\xi_{tj} + X_t^{\wedge}(k-1) \tag{22}$$

where the cubature points set $\xi_{tj} = \sqrt{h/2}[1]_{tj}$, $[1]_{tj}$ represents the *j*th element of the cubature point sets, *h* is the total cubature point. When using third-order cubature principle, the total cubature point of *h* is twice the number of state dimensional *e*, *i* = 1, 2, …, *e*, *j* = 1, 2…*h*. Among of the parameter variables, *e* = 3, the cubature point set as follows:

$$\left\{ \begin{bmatrix} 1 \\ 0 \\ 0 \end{bmatrix}, \begin{bmatrix} 0 \\ 1 \\ 0 \end{bmatrix}, \begin{bmatrix} 0 \\ 0 \\ 1 \end{bmatrix}, \begin{bmatrix} -1 \\ 0 \\ 0 \end{bmatrix}, \begin{bmatrix} 0 \\ -1 \\ 0 \end{bmatrix}, \begin{bmatrix} 0 \\ 0 \\ -1 \end{bmatrix} \right\}$$

② The cubature point $X_{tj}^*(k/k-1)$

$$X_{tj}^*(k/k-1) = f(X_{tj}(k/k-1)) \tag{23}$$

③ The parameter variables $X_t^{\wedge}(k/k-1)$

$$X_t^{\wedge}(k/k-1) = \sum_{j=1}^{h} \frac{1}{h} X_{tj}^*(k/k-1) \tag{24}$$

④ The error covariance matrix $P_t(k/k-1)$

$$P_t(k/k-1) = \sum_{j=1}^{h} \frac{1}{v} \omega_{tj} X_{tj}^*(k/k-1) X_{tj}^{*T}(k/k-1) - X_t^{\wedge}(k/k-1) X_t^{\wedge T}(k/k-1) + Q_t \tag{25}$$

(3) Time update of vehicle state estimator

① To factorise the covariance matrix $P_s(k-1)$ based on SVD

$$P_s(k-1) = A_s(k-1)\Lambda_s(k-1)A_s^T(k-1) \tag{26}$$

$$\Lambda_s(k-1) = diag[S_{s,1}^2, S_{s,2}^2 ....., S_{s,n}^2]$$

where the row of the $A_s(k-1)$ is unit orthogonal feature vector of error covariance $P_s(k-1)$, $\Lambda_s(k-1)$ is diagonal matrix, $S_{s,i}$ are eigen values of the error covariance matrix $P_s(k-1)$.

$$X_s(j,k-1) = A_s(i,k-1)S_s(i,k-1)\xi_{s,j} + X_s^{\wedge}(k-1) \tag{27}$$

where the cubature points $\xi_{sj} = \sqrt{m/2}[1]_{sj}$, $[1]_{sj}$ represents the *j*th element of the cubature point sets, *m* is the total cubature point, *n* is the state dimension. When using third-order cubature principle, the total cubature point of *m* is twice the number of state dimensional *n*, *i* = 1, 2…*n*, *j* = 1, 2…*m*. Among of the parameter variables, *n* = 6, the cubature point set as follows:

$$\left\{\begin{bmatrix}1\\0\\0\\0\\0\\0\end{bmatrix},\begin{bmatrix}0\\1\\0\\0\\0\\0\end{bmatrix},\begin{bmatrix}0\\0\\1\\0\\0\\0\end{bmatrix},\begin{bmatrix}0\\0\\0\\1\\0\\0\end{bmatrix},\begin{bmatrix}0\\0\\0\\0\\1\\0\end{bmatrix},\begin{bmatrix}0\\0\\0\\0\\0\\1\end{bmatrix},\begin{bmatrix}-1\\0\\0\\0\\0\\0\end{bmatrix},\begin{bmatrix}0\\-1\\0\\0\\0\\0\end{bmatrix},\begin{bmatrix}0\\0\\-1\\0\\0\\0\end{bmatrix},\begin{bmatrix}0\\0\\0\\-1\\0\\0\end{bmatrix},\begin{bmatrix}0\\0\\0\\0\\-1\\0\end{bmatrix},\begin{bmatrix}0\\0\\0\\0\\0\\-1\end{bmatrix}\right\}$$

② The cubature point $X_s^*(j,k/k-1)$

$$X_s^*(j,k/k-1)=f(X_s(j,k/k-1),X_p^{\wedge}(k/k-1),X_t^{\wedge}(k/k-1),U_k)\quad j=1,2\ldots m \tag{28}$$

③ The state variables $X_s^{\wedge}(k/k-1)$

$$X_s^{\wedge}(k/k-1)=\sum_{j=1}^{m}\frac{1}{m}X_s^*(j,k/k-1) \tag{29}$$

④ Prediction of error covariance $P_s(k/k-1)$

$$P_s(k/k-1)=\sum_{j=1}^{m}\omega_j X_s^*(j,k/k-1)X_s^{*T}(j,k/k-1)-X_s^{\wedge}(k/k-1)X_s^{\wedge T}(k/k-1)+Q_s \tag{30}$$

(4) Measurement update of vehicle state estimation

① To factorise the error covariance matrix $P_s(k/k-1)$ based on SVD

$$\begin{aligned}&P_s(k/k-1)=A_{k/k-1}\Lambda_{k/k-1}A_{k/k-1}^T\\&X_s(j,k/k-1)=A_s(i,k/k-1)S_s(i,k/k-1)\xi_{s,j}+X_s^{\wedge}(k/k-1)\\&\qquad i=1,2\ldots n\ \ j=1,2\ldots m\end{aligned} \tag{31}$$

② The cubature point $Z_s(j,k/k-1)$

$$Z_s(j,k/k-1)=h(X_s(j,k/k-1)) \tag{32}$$

③ The mean of measured variables $Z_s^{\wedge}(k/k-1)$

$$Z_s^{\wedge}(k/k-1)=\sum_{j=1}^{m}\frac{1}{m}Z_s(j,k/k-1) \tag{33}$$

④ The innovation covariance $P_{zz,s}(k/k-1)$

$$P_{zz,s}(k/k-1)=\sum_{j=1}^{m}\frac{1}{m}Z_g(j,k/k-1)Z_s^T(j,k/k-1)-Z_s^{\wedge}(k/k-1)Z_s^{\wedge T}(k/k-1)+R_s \tag{34}$$

⑤ The cross-covariance $P_{xz,s}(k/k-1)$

$$P_{xz,s}(k/k-1)=\sum_{j=1}^{m}\frac{1}{m}X_s(j,k/k-1)Z_s^T(j,k/k-1)-X_s^{\wedge}(k/k-1)Z_s^{\wedge T}(k/k-1) \tag{35}$$

⑥ The gain matrix $K_s(k)$

$$K_s(k) = P_{xz,s}(k/k-1)P_{zz,s}^{-1}(k/k-1) \tag{36}$$

⑦ State estimates value $X_s^{\wedge}(k)$

$$X_s^{\wedge}(k) = X_s^{\wedge}(k/k-1) + K_s(k)[Z_s(k) - Z_s^{\wedge}(k/k-1)] \tag{37}$$

⑧ The error covariance matrix $P_s(k)$

$$P_s(k) = P_s(k/k-1) - K_s(k)P_{zz,s}(k/k-1)K_s^T(k) \tag{38}$$

(5) Measurement update of road friction coefficient estimation

① To factorise the error covariance $P_p(k/k-1)$ matrix based on SVD

$$\begin{aligned} &P_p(k/k-1) = A_p(i,k/k-1)\Lambda_p(k/k-1)A_p^T(k/k-1) \\ &X_p(j,k/k-1) = A_p(i,k/k-1)S_p(i,k/k-1)\xi_{p,j} + X_p^{\wedge}(k/k-1) \\ &\qquad i = 1,2\ldots M,\ j = 1,2\ldots\ldots,N \end{aligned} \tag{39}$$

② The cubature point $Z_{pj}(k/k-1)$

$$Z_{pj}(k/k-1) = h(X_{pj}(k/k-1), X_t^{\wedge}(,k/k-1), X_s^{\wedge}(k), U_k) \tag{40}$$

③ The measuring mean value $Z_p^{\wedge}(k/k-1)$

$$Z_p^{\wedge}(k/k-1) = \sum_{j=1}^{M} \frac{1}{M} Z_{pj}(k/k-1) \tag{41}$$

④ The innovation covariance matrix $P_{zz,P}(k/k-1)$

$$P_{zz,p}(k/k-1) = \sum_{j=1}^{M} \frac{1}{M} Z_{pj}(k/k-1)Z_{pj}^T(k/k-1-Z_p^{\wedge}(k/k-1)Z_p^{\wedge T}(k/k-1) + R_p \tag{42}$$

⑤ The cross-covariance matrix $P_{xz,p}(k/k-1)$

$$P_{xz,p}(k/k-1) = \sum_{j=1}^{M} \frac{1}{M} X_{pj}(k/k-1)Z_{pj}^T(k/k-1) - X_p^{\wedge}(k/k-1)Z_p^{\wedge T}(k/k-1) \tag{43}$$

⑥ The gain matrix $K_p(k)$

$$K_p(k) = P_{xz,p}(k/k-1)P_{zz,p}^{-1}(k/k-1) \tag{44}$$

⑦ The parameters variables $X_p^{\wedge}(k)$

$$X_p^{\wedge}(k) = X_p^{\wedge}(k/k-1) + K_p(k)(Z_p(k) - Z_p^{\wedge}(k/k-1)) \tag{45}$$

⑧ The error covariance matrix $P_p(k)$

$$P_p(k) = P_p(k/k-1) - K_p(k)P_{zz,p}(k/k-1)K_p^T(k) \tag{46}$$

(6) Measurement update of vehicle parameters estimator

① To factorise the error covariance matrix $P_t(k/k-1)$ based on SVD

$$P_t(k/k-1) = A_t(i,k/k-1)\Lambda_t(k/k-1)A_t^T(k/k-1)$$
$$X_t(j,k/k-1) = A_t(i,k/k-1)S_t(i,k/k-1)\xi_{t,j} + X_t^{\wedge}(k/k-1) \quad (47)$$
$$i = 1,2\ldots,e,\ j = 1,2\ldots,h$$

② The cubature point $Z_{tj}(k/k-1)$

$$Z_{tj}(k/k-1) = h(X_{tj}(k/k-1), X_p^{\wedge}(k), X_s^{\wedge}(k), U_k) \quad (48)$$

③ Mean value of measured variables $Z_t^{\wedge}(k/k-1)$

$$Z_t^{\wedge}(k/k-1) = \sum_{j=1}^{h}\frac{1}{h}Z_{tj}(k/k-1) \quad (49)$$

④ The innovation covariance matrix $P_{zz,t}(k/k-1)$

$$P_{zz,t}(k/k-1) = \sum_{j=1}^{h}\frac{1}{h}Z_{tj}(k/k-1)Z_{tj}^T(k/k-1) - Z_t^{\wedge}(k/k-1)Z_t^{\wedge T}(k/k-1) + R_t \quad (50)$$

⑤ The cross-covariance matrix $P_{xz,t}(k/k-1)$

$$P_{xz,t}(k/k-1) = \sum_{j=1}^{h}\frac{1}{h}X_{tj}(k/k-1)Z_{tj}^T(k/k-1) - X_t^{\wedge}(k/k-1)Z_t^{\wedge T}(k/k-1) \quad (51)$$

⑥ The gain matrix $K_t(k)$

$$K_t(k) = P_{xz,t}(k/k-1)P_{zz,t}^{-1}(k/k-1) \quad (52)$$

⑦ The parameters variables $X_t^{\wedge}(k)$

$$X_t^{\wedge}(k) = X_t^{\wedge}(k/k-1) + K_t(k)(Z_t(k) - Z_t^{\wedge}(k/k-1)) \quad (53)$$

⑧ The error covariance matrix $P_t(k)$

$$P_t(k) = P_t(k/k-1) - K_t(k)P_{zz,t}(k/k-1)K_t^T(k) \quad (54)$$

where Q_g, Q_p and Q_t are process noise covariance matrix, R_g, R_p and R_t are measurement noise covariance matrix.

The state variables of vehicle state estimator:

$$X_s = [u, v, \gamma, a_x, a_y, \Gamma]$$

The parameter variables of tyre-road friction coefficient estimation:

$$X_p = [\mu_{fl}, \mu_{fr}, \mu_{rl}, \mu_{rr}]$$

The parameter variables of vehicle parameters estimator:

$$X_t = [m, I_z, a]$$

The control input variables of vehicle driving state and parameter estimator:

$$u_k = [\delta, \omega_{ij}]$$

The measured variables of vehicle state estimator:

$$Z_s = [a_x, a_y, \gamma]$$

The measured variables of tyre-road friction coefficient estimation:

$$Z_p = [a_x, a_y, \dot{\gamma}]$$

The measured variables of vehicle parameters estimator:

$$Z_t = [a_y, \dot{\gamma}]$$

4 Experiment verification based on driving simulator

According to the driving simulator in-loop experiment, the estimation algorithm for vehicle driving state and parameters proposed in the paper is verified.

4.1 Driving simulator experiment platform

The driving simulator experiment platform is shown in Figure 2. It includes host computer (upper computer), dSPACE data processor (lower computer), data collector, operation platform, audio equipment, fusion machine and projector etc. The programs in host computer (upper computer) are transition to code through building, and the code is downloaded to lower computer. The vehicle model and estimation procedures are running in real-time through the dSPACE data processor. At the same time, the driver's handling signals are received from the data collector, to calculate the response of vehicle motion and estimate. The operation result, vehicle driving state can be dynamic displayed by the screen of operation platform and the ring screen respectively. In the loop experiment, the simulation sound of engine and braking can be issued form audio equipment when vehicle running. The image that three projector generated can be displayed in ring screen by fusion machine.

The estimation algorithm program is written through using Matlab/Simulink. A vehicle model (front-engine and front-drive transmission system) is chosen in driving simulator in real-time simulation software CarSim. The estimate principle is shown in Figure 3. The part parameters of the vehicle model are shown in Table 1.

Table 1 Part parameters of vehicle model

Variable parameters	*Symbol*	*Value*
Vehicle mass (kg)	m	1231
The rotational inertia of the z-axis (kg.m^2)	I_z	2031
Distance from centre of mass to front axle (m)	a	1.04
Front and rear wheelbase(m)	L	2.6
Centroid height (m)	h	0.54
Wheel track of the front wheel (m)	t_f	1.481
Wheel track of the rear wheel (m)	t_r	1.486
Effective radius of wheel (m)	R_e	0.31
Steering gear ratio	i	18

Figure 2 Driving simulator composition diagram (see online version for colours)

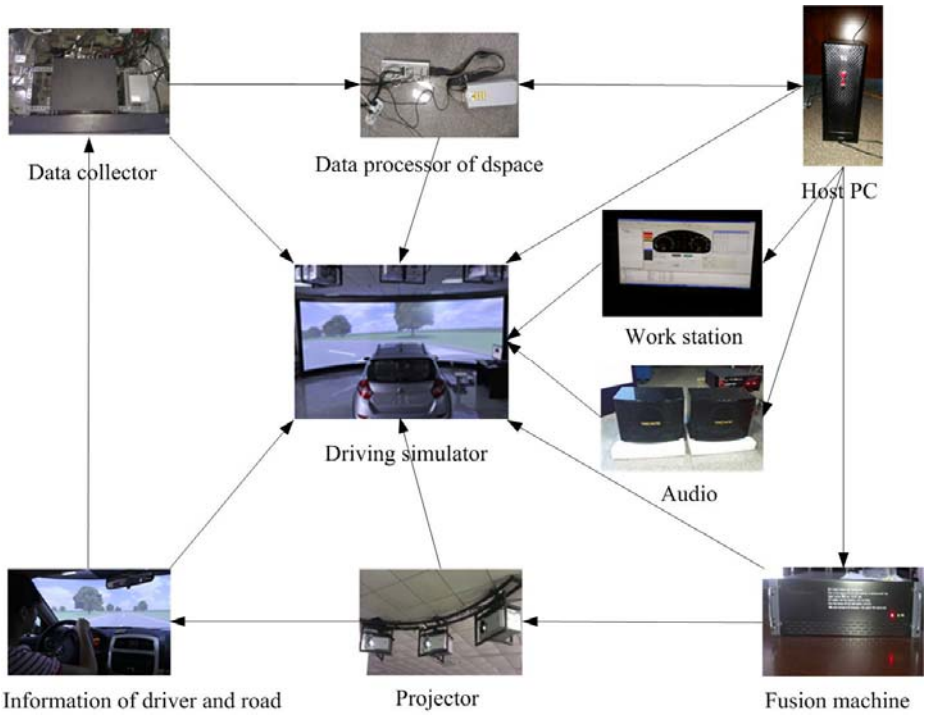

Figure 3 Estimation principle of driving simulator in-loop experiment (see online version for colours)

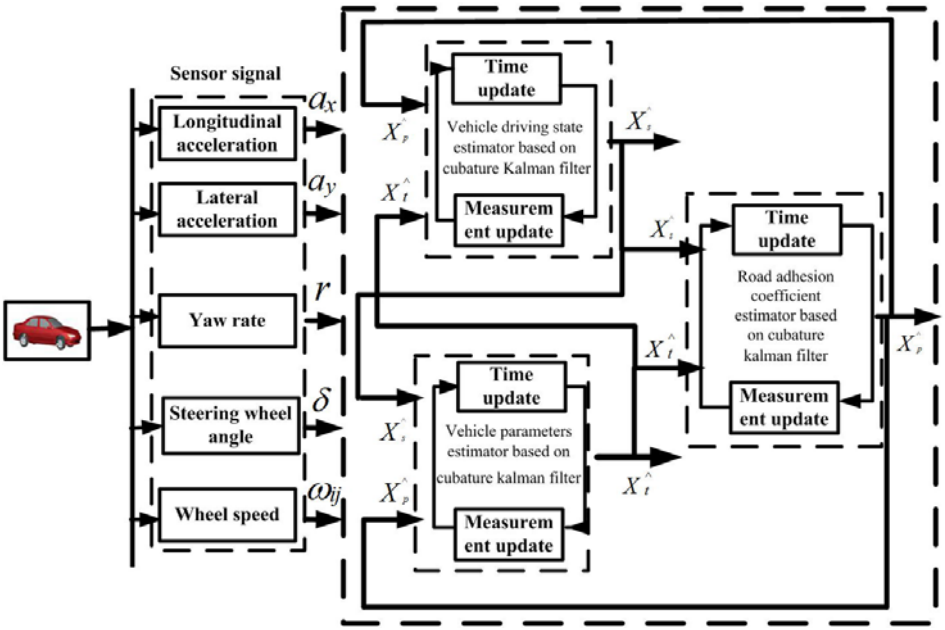

The theory of driving state and parameters estimation algorithm based on triple CKF is shown in Figure 3, $X_s^{\wedge}$ is the vehicle driving state, it includes vehicle longitudinal/lateral velocity and yaw acceleration etc. $X_t^{\wedge}$ are parameter variables, consisting of the vehicle mass, the rotational inertia of the z-axis and the distance from the centre of vehicle mass to front axle. The parameters variables $X_p^{\wedge}$ are composed of road adhesion coefficients. At the initial time, the first initial values of the process noise matrix Q_s, Q_p and Q_t, the error noise covariance matrix P_s, P_p and P_t, the state variable $X_s^{\wedge}$, the parameters variables $X_p^{\wedge}$ and $X_t^{\wedge}$, and the measurement noise covariance matrix R_s, R_p and R_t should be given.

Figure 4 The sensor signals: (a) longitudinal acceleration signal; (b) lateral acceleration signal; (c) yaw rate signal; (d) steering wheel angle signal and (e) wheel speed signal (see online version for colours)

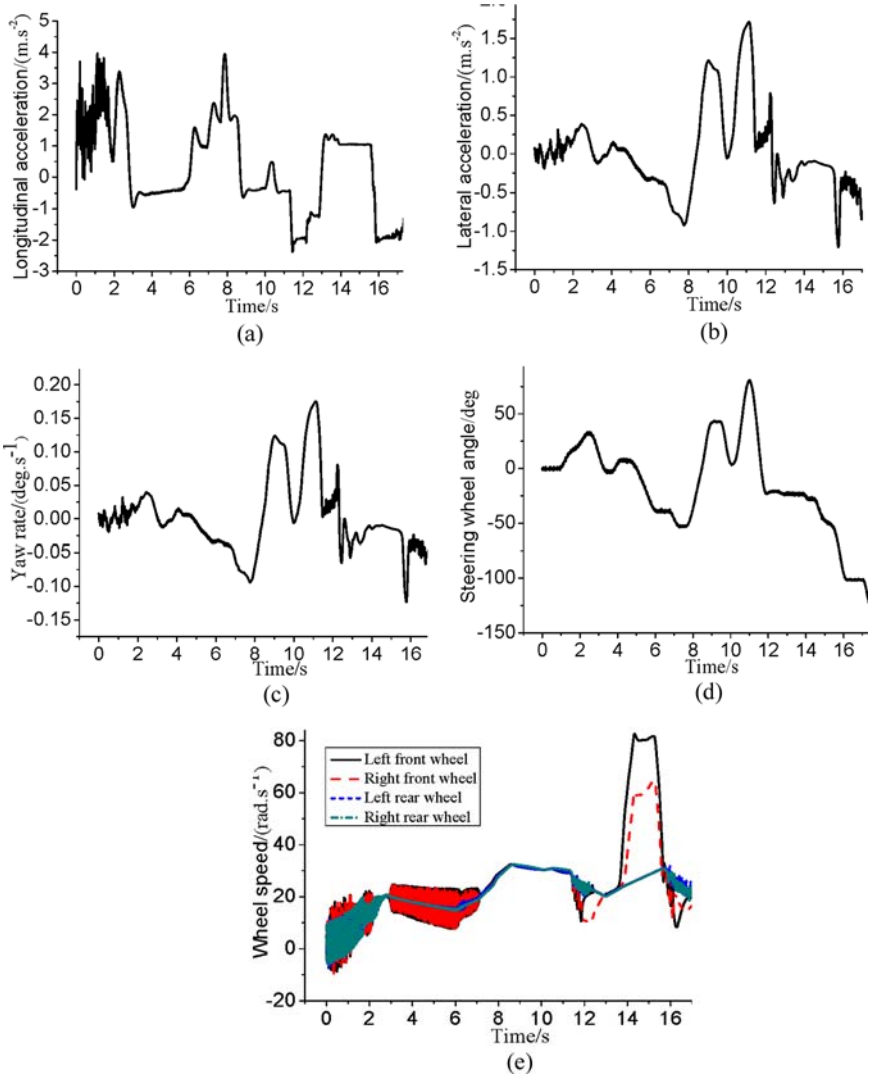

Figure 5 Contrast curves of driving estimator in-loop experiment: (a) longitudinal velocity; (b) lateral speed; (c) side-slip angle; (d) road adhesion coefficient; (e) vehicle mass; (f) moment of inertia about *z*-axis and (g) centroid position (see online version for colours)

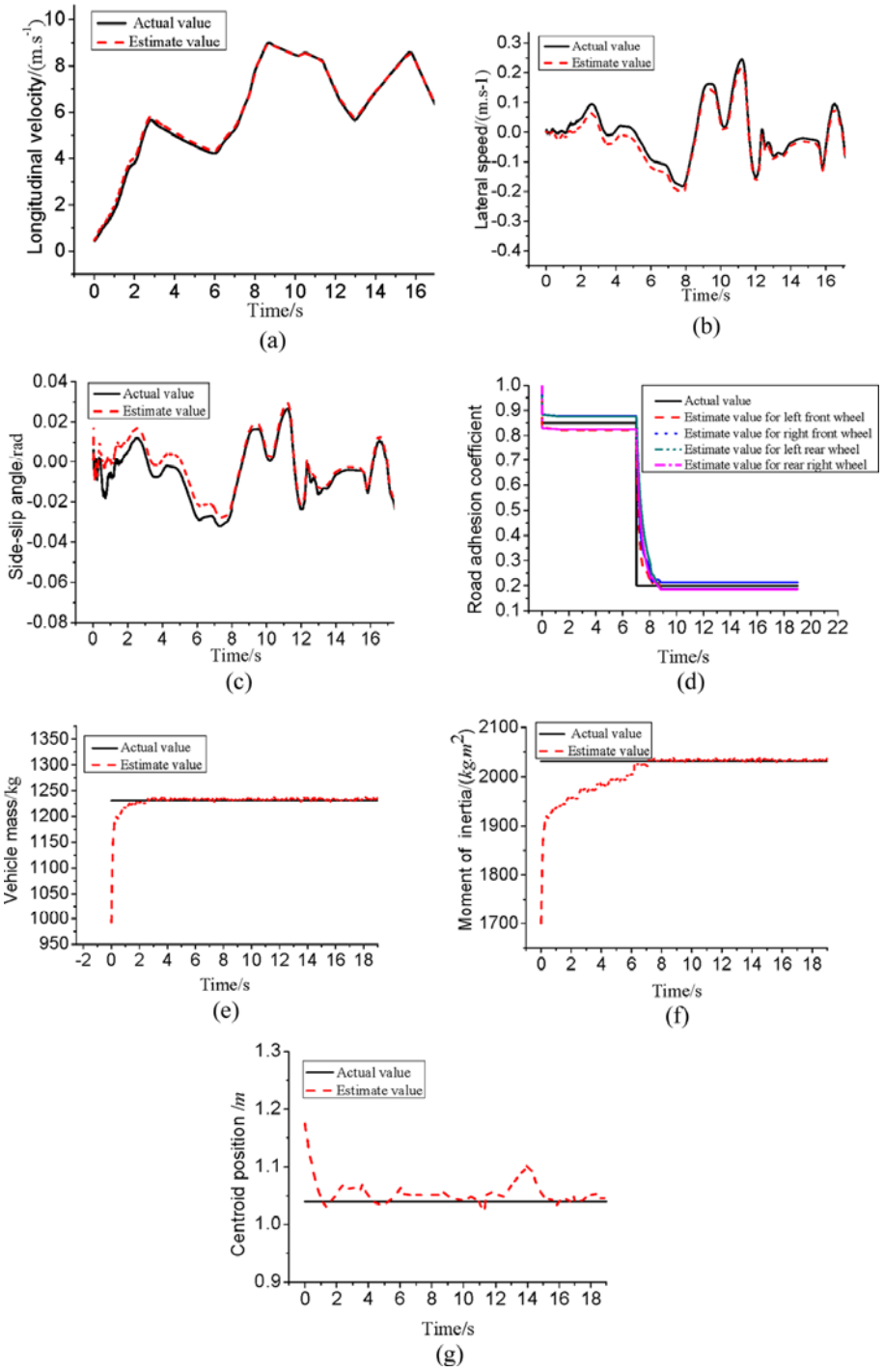

The driving state and parameters estimator are based on the triple CKF. For vehicle driving state and parameters estimator, the inputs are sensor signals such as the vehicle longitude/lateral acceleration, yaw rate, steering wheel angle and wheel speed. For road adhesion coefficient estimator, the inputs are vehicle sensor signals, vehicle driving state and vehicle parameters (the vehicle mass, moment of inertia and centroid position). Nonlinear 3-DOF model and Dugoff tyre model are established. Finally, the estimation for road adhesion coefficient is realised through triple CKF theory. For vehicle parameters estimator, the inputs are vehicle sensor signals, vehicle driving state and tyre-road friction coefficient, and the estimation for vehicle parameters is realised through triple CKF theory. For the vehicle driving state estimator, the inputs are vehicle's sensor signals, tyre-road friction coefficient and vehicle parameters, and the estimation for vehicle driving state is realised through triple CKF theory. Then, the triple CKF estimator is established by combining with the vehicle state estimator, road adhesion coefficient estimator and vehicle parameters estimator. So those estimated pieces of information can correct each other through triple CKF theory, and the vehicle state and parameters can be accurately estimated.

4.2 Experiment condition

To verify the validity of the driving state and parameters estimation algorithm based on triple CKF, the serpentine docking road conditions with changing speed are selected in driving simulator hardware in-loop experiment.

Serpentine docking road conditions with changing speed are as follows: at first 7 s, the road adhesion coefficient is 0.85; at last 12 s, the road adhesion coefficient becomes 0.2; the sampling interval is 0.005 s. The initial values of driving state estimator are set as follows: the state variable X_s = [0.46509, 0.000433744, 0, 0, 0, 0], the error covariance matrix P_s = eye(6)*10000, the measurement noise covariance matrix R_s = eye(3)*3, and the process noise covariance matrix Q_s = eye(6)*3. The parameters of road adhesion coefficient estimator are set as follows: the parameter variable X_p = [1, 1, 1, 1], the error covariance matrix P_p = [1, 0, 0, 0; 0, 0.8, 0, 0; 0, 0, 0.8, 0; 0, 0, 0, 0.9]*500, the process noise covariance matrix Q_p = eye(4)*0.0001, the measurement noise covariance matrix R_p = [0.01, 0, 0; 0, 1, 0; 0, 0, 0.1]*1000. The initial values of vehicle parameters estimator are set as follows: the parameter variable X_t = [1000, 1700, 1.2], the error covariance matrix P_t = [10, 0, 0; 0, 10, 0; 0, 0, 10]*0.007, the process noise covariance matrix Q_t = [1, 0, 0; 0, 1, 0; 0, 0, 1]*1, and the measurement noise covariance matrix Rt = [1, 0; 0, 1]*1.

The analysis for the results of driver simulator in-loop experiment are as follows: Figures 4(a)–(e) are the sensor signals of simulation vehicle; Figure 5 shows the contrast curves of driving simulator hardware in-loop experiment; Figure 5(a) is the contrast curve of estimate value and experimental value for longitudinal velocity. From the figure, it can be seen that the estimate values are very close to the experimental values, their maximum error is about 1%. Figure 5(b) is the contrast curve for estimate value and experimental value of lateral speed. From the figure, it can be seen that the estimate values are very close to the experimental values, their maximum error is about 5%. Figure 5(c) is the contrast curve for estimate value and experimental value of side-slip angle. From the figure, the estimate values are very close to the experimental values, their maximum error is about 5%. Figure 5(a)–(c) show that the estimate values delay time is about 0.005 s, therefore, the real-time performance is very good. Figure 5(d) is the contrast curve for

estimate value and experimental value of road adhesion coefficient. From the figure, it can be seen that the estimate values can convergence to the actual value quickly. The final road adhesion coefficient can be determined through using weighted average method on real vehicle. Figure 5(e) is the contrast curve for estimate value and experimental value of vehicle mass. From the figure, it can be seen that the estimate values can convergence to the actual value quickly, and the precision is very high. Figure 5(f) is the contrast curve of estimate value and experimental value for the moment of inertia about *z*-axis. From the figure, it can be seen that the estimate values can convergence to the actual value quickly with high precision and better stability. Figure 5(g) is the contrast curve of estimate value and experimental value for the centroid position. From the figure, it can be seen that the estimate values can convergence to the actual value quickly, and the estimate values always bounce near the actual value with high precision and better stability.

5 Conclusion

1 The nonlinear 3-DOF vehicle model with Dugoff tyre model is established in the paper. Based on the CKF theory, the vehicle longitudinal and lateral speeds, side-slip angle and other state variables are estimated through sensor information. At the same time, through using state estimation and sensor information, the estimates for the road friction coefficient and vehicle mass, the moment of inertia about *z*-axis and the centroid position are realised.

2 Considering the actual driving environment, the road adhesion conditions, the vehicle mass, the moment of inertia about *z*-axis and the centroid position will affect the state estimation. So the vehicle state estimator and the variable parameters estimator are combined with each other, in order to realise the accurate estimation for driving state and parameters.

3 Through the driving simulator in-loop experiment, the vehicle driving state and parameters estimation algorithm are verified. The results indicated that the algorithm can accurately estimate the vehicle state and parameters.

Acknowledgements

The work is supported by National Science Foundation of China (51675257, 51305190), Project of Liaoning Province Innovative Talents (LR2016054), and Project of Liaoning Province major science and technology platform (JP2016003, 2017001).

References

Antonova, S., Fehn, A. and Kugi, A. (2011) 'Unscented Kalman filter for vehicle state estimation', *Vehicle System Dynamics*, Vol. 49, No. 9, pp.1497–1520.

Arasaratnam, I., Haykin, S. and Hurd, T.R. (2009) 'Cubature Kalman filters', *IEEE Trans. on Automatic Control*, Vol. 54, No. 6, pp.1254–1269.

Arasaratnam, I., Haykin, S. and Hurd, T.R. (2010) 'Cubature Kalman filtering for continuous-discrete systems: theory and simulations', *IEEE Trans. on Signal Processing*, Vol. 58, No. 10, pp.4977–4993.

Baffet, G., Charara, A. and Dherbomez, G. (2007) 'An observer of tire-road forces and friction for active security vehicle system', *IEEE/ASME Transactions on Mechatronics*, Vol. 12, No. 6, pp.651–661.

Best, M.C. (2009) 'Identifying tyre models directly from vehicle test data using an extended Kalman filter', *Vehicle System Dynamics*, Vol. 48, No. 2, pp.171–187.

Choi, M., Oh, J.J. and Choi, S.B. (2013) Linearized recursive least squares methods for real time identification of tire-road friction coefficient', *IEEE Transactions on Vehicular Techonology*, Vol. 62, No. 7, pp.2906–2918.

Crassidis, J.L. and Markley, F.L. (2003) 'Unscented for spacecraft attitude estimation', *Journal of Guidance Control and Dynamics*, Vol. 26, No. 4, pp.536–542.

Givon, D., Stinis, P. and Weare, J. (2009) 'Variance reduction for particle filters of systems with time scale separation', *IEEE Trans. on Signal Processing*, Vol. 57, No. 2, pp.424–435.

Grip, H.F., Imsland, L., Johansen, T.A., Fossen, T.I., Kalkkuhl, J.C. and Suissa, A. (2008) 'Nonlinear vehicle side-slip estimation with friction adaptation', *Automatica*, Vol. 44, No. 3, pp.611–622.

Gustafsson, F., Gunnarsson, F., Bergman, N., Forssell, U., Jansson, J., Karlsson, R. and Nordlund, P-J. (2002) 'Particle filters for positioning, navigation and tracking', *IEEE Trans on Signal Processing*, Vol. 50, No. 2, pp.425–437.

Gust, A.F. (2010) 'Particle filters theory and practice with positioning applications', *IEEE Aerospace and Electronic Systems Magazine*, Vol. 25, No. 7, pp.53–82.

Julier, S.J. and Uhlman, J.K. (2004) 'Unscented filtering and nonlinear estimation', *Proceedings of the IEEE*, Vol. 92, No. 3, pp.401–422.

Julier, S.J., Uhlman, J.K. and Durrant-Whyte, H.F. (2000) 'A new method for the nonlinear transformation of means and covariances in filters and estimators', *IEEE Transactions on Automatic Control*, Vol. 45, No. 3, pp.477–482.

Kandepu, R. and Foss, B. (2008) 'Applying the unscented Kalman filter for nonlinear state estimation', *Journal of Process Control*, Vol. 11, No. 4, pp.753–768.

Kim, J. (2009) 'Identification of lateral tyre force dynamics using an extended Kalman filter from experimental road test data', *Control Engineering Practice*, Vol. 17, No. 3, pp.357–367.

Li, Q. and Sun, F. (2013) 'Adaptive cubature particle filter algorithm', *IEEE International Conference on Mechatronics and Automation*, Vol. 7, No. 4, pp.1355–1360.

Nam, K. and Fujimoto, H. (2012) 'Estimation of sideslip and roll angles of electric vehicles using lateral tire force sensors through RLS and Kalman filter approaches', *IEEE Transactions on Vehicular Techonology*, Vol. 61, No. 5, pp.1792–1785.

Pengov, M., d'Andréa-Novel, B. and Fenaux, E. (2001) 'A comparison study of two kinds of observers for a vehicle', *Proceedings of the European Control Conference*, Porto, September, pp.1068–1073.

Phanomchoeng, G., Rajamani, R. and Piyabongkarn, D. (2011) 'Nonlinear observer for bounder Jacobian systems with applications to automotive slip angle estimation', *IEEE Transactions on Automatic Control*, Vol. 56, No. 5, pp.1163–1170.

Satria, M. and Best, M.C. (2005) *Comparison between Kalman Filter and Robust Filter for Vehicle Handling Dynamics State Estimation*, SAE Tech. Pap. Series, No. 2005-01-11850.

Van Der Merwe, R., Wan, E.A. and Julier, S.I. (2004) 'Sigma-point Kalman filters for nonlinear estimation and sensor-fusion-applications to integrated navigation', *Proceedings of the AIAA Guidance, Navigation & Control Conference (GNC)*, AIAA-2004-5120, August, Providence, Rhode Island, pp.1735–1764.

Wenzel, T.A., Burnham, K.J. and Blundell, M.V. (2006) 'Dual extended Kalman filter for vehicle state and parameter estimation', *Vehicle System Dynamics*, Vol. 44, No. 2, pp.153–171.

Wilkin, M.A., Crolla, D.C. and Levesley, M.C. (2006) *Designed Verification of an Extended Kalman Filter to Estimation Vehicle Tyre Force*, SAE Paper 2006-01-1285.

Zong, C-F., Song, P. and Hu, D. (2011) 'Estimation of vehicle states and tire-road friction using parallel extended Kalman filtering', *Journal of Zhejiang University-SCIENCE A (Applied sPhysics & Engineering)*, Vol. 12, No. 6, pp.446–452.